Institute of Space and Aeronautical Science, University of Tokyo
Report No. 523, March 1975

Stress Analysis of a Concave Polyhedral Shell*

By

Kazuo TANIZAWA and Koryo MIURA

Summary: The stress analysis of the PCCP shell, which is a kind of concave polyhedral shells, is presented. Both the numerical method (FEM) and the experimental method are used in the analysis. Resultantly, the elastic behaviour and stress distributions of the PCCP shell subjected to either axial compression or hydrostatic pressure are made clear. The higher buckling pressures of PCCP shells in comparison with that of the circular cylinder are obtained experimentally. Besides, it was found that the particular stress distribution observed in PCCP shells in axial compression gave a basis for Miura's hypothesis to explain the collapsing mechanism of general cylindrical shells.

Nomenclature

E	Young's modulus
E_e	equivalent axial stiffness
N	circumferential wave number
P	axial load
R	radius of the circumcylinder
a	half length of a valley line
b	height of a triangular element
l	axial length of the *PCCP* shell
p	external pressure
r	ratio of the axial component of the external pressure to the one of the hydrostatic pressure
t	shell wall thickness
u	displacement
x, y	local rectangular coordinates
r, θ, y	global cylindrical coordinates
σ_a, σ_θ	axial and hoop stresses in cylindrical coordinates
σ_m, σ_b	membrane and bending stress
σ_{ae}, σ_{pe}	reference stresses $\sigma_{ae}=P/(2\pi Rt)$, $\sigma_{pe}=pR/t$
δ	displacement occured by the external load
ν	Poisson's ratio

* The part of this paper was presented as a partial fulfillment of the requirements for the Master's Degree for the first author at the University of Tokyo, March 1973.

Subscript

- a axial quantity
- b bending quantity
- f quantity related to fracture
- m membrane quantity
- θ circumferential quantity

1. Introduction

The concept of the pseudo cylindrical polyhedral shell (*PCCP* shell) has been proposed by Miura [*1*], [*2*] a several years ago. It is the shell whose shape resembles the post-buckled configuration (Yoshimura-pattern) of a thin circular cylindrical shell. More exactly, the midsurface of the shell is the surface obtained by uniformly axial shortening of a cylindrical surface through an isometric transformation. The *PCCP* shells, whose overall configurations are cylindrical, are characterized by high circumferential bending rigidity and low axial rigidity in comparison with the cylindrical shell of similar dimensions. In other words, *PCCP* shells can be considered as the inherently circumferentially stiffened cylindrical shells. In spite of the useful properties of the *PCCP* shell, the structural analysis of it has not been performed until recently. However, the need for the analysis of the *PCCP* shell was envisaged recently in two quite different fields of engineering, that is, the automobile engineering and ocean engineering.

In the automobile engineering, the tubular column type collapsible shock energy absorber is extensively studied for designing the safer car in head-on collision. In the process of collapsing, a cylindrical shell experiences first the post-buckling regime which is described geometrically as the *PCCP* surface and then goes into total collapsing. Therefore, the study of energy absorbed and the shock load-deformation relation can not be performed without the knowledge of the stress analysis of *PCCP* shells.

In the field of ocean engineering, Knapp [*3*] proposed the use of the *PCCP* shell for shallow undersea habitats. The idea of it rests on the facts that the *PCCP* shell has the inherent high circumferential bending rigidity, it is a near cylindrical form, it can be constructed from the many identical triangular flat panels, and so forth. Since the structural design criteria of such structures is most likely the buckling under the hydrostatic pressure rather than the material strength, *PCCP* shells are probably favorable. This is the reason why the investigation of stress and stability analysis of *PCCP* shells under hydrostatic pressure is necessary.

Thus, we have performed both experimental and numerical analyses of the behaviour of *PCCP* shells. The loading conditions considered are the axial compression, hydrostatic pressure and lateral pressure. The stress analyses are performed both experimentally and numerically for all of the above loadings. The stability analysis is performed experimentally in the case of hydrostatic pressure.

2. Outline of Model Experiments

2-1 Method of Making *PCCP* Shell Models

The primary purpose of this model experiment is to obtain the knowledge about the stress distribution of the *PCCP* shell subject to a certain load. The preliminary experimental survey of the shell using photoelastic models revealed that the higher stresses exist in the region along ridges. Therefore, the model must be accurately made especially in ridge regions and the discontinuity, such as bonding line, must be kept minimum.

For these reasons, we have decided to make the models through the vacuum forming of *HIPS* (High Impact Polystylene) cylinders at temperature about 210°C. The said cylinder is made of a sheet of *HIPS* of 1 mm thick by rolling and lap bonding at a seam line along its axis. The radius of the cylinder is so designed as to coincide with the radius of the circumcylinder of the *PCCP* shell. The original circular cylinder thus made is also used as the specimen subject to hydrostatic pressure for the purpose of comparison.

The *PCCP* shell models having six ($N=6$) and eight ($N=8$) circumferential wave numbers were made. The thickness of a typical triangular element was measured in detail. It was observed that in general the wall thickness decreases in concave parts and increases in convex parts whose deviation from the average value is at most 10% in models of $N=6$ and $N=8$.

2-2 Test Procedure

Since the material properties of *HIPS* will change after the vacuum forming at moderately high temperature, some strips of *HIPS* sheet were put into the same furnace and the change of them were measured and listed in Table 1. In order to know the mechanism of the transmission of the load in *PCCP* shells, we pasted strain gages on some element surfaces. Taking into account the hardening effect of the strain gage and taking advantage of symmetry of *PCCP* shells, we scattered positions of strain gages on three element surfaces. Fig. 2 shows one *PCCP* shell in experiment and Fig. 3 shows the geometrical features of two models.

As to the loading conditions, the hydrostatic pressure and the axial compression were adopted. The former corresponds to the case of underwater structure and the latter to the controllable collapsing structure. In both cases, the total axial shorten ing was measured by four dial gages so as to know the macroscopic mechanical property of a *PCCP* shell in comparison with a circular cylinder.

Table 1

	Original Cylinder	*PCCP* shells
Young's modulus	315.4 Kg/mm²	252.2 Kg/mm²
Poisson's rate	0.316	0.311

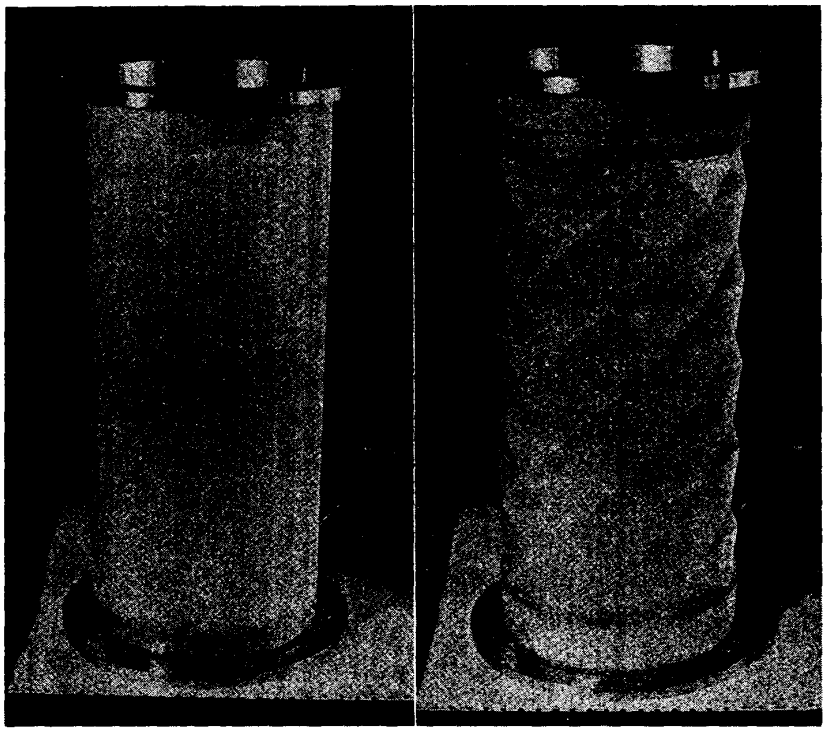

FIG. 1. Original circular cylinder and PCCP shell.

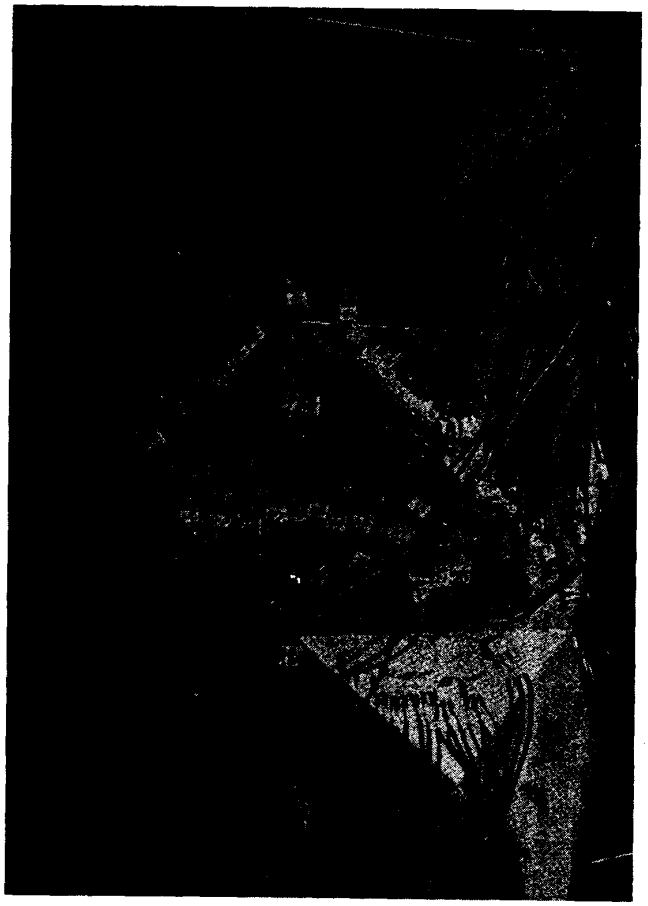

FIG. 2. Test piece in experiment.

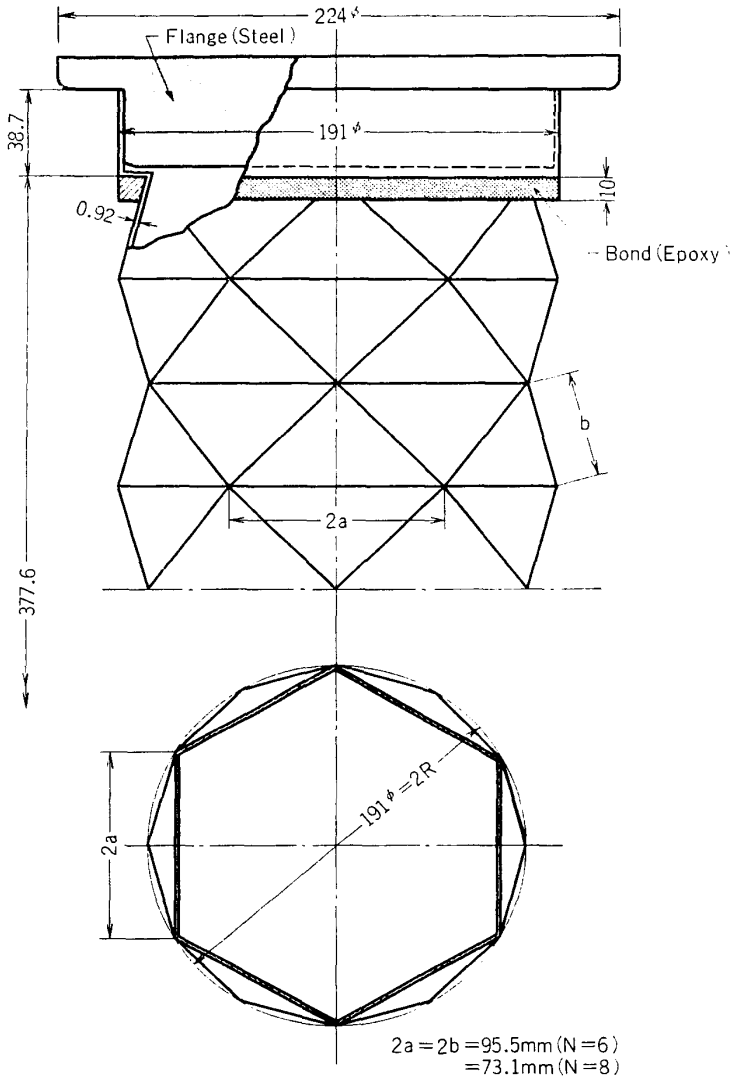

FIG. 3. Geometrical features of PCCP shell models.

3. OUTLINE OF NUMERICAL ANALYSIS

Numerical analysis was performed by the finite element displacement method in elastic linear region. In this method, the most important thing is to select the good shape function. Therefore, we used the well-known two shape functions for bending which had been investigated very well. One is a nonconforming function by Bazeley et al [*4*] and the other is a conforming function by Clough and Tocher [*5*]. As an in-plane shape function, we used the linear polynomial for both cases.

As far as *PCCP* shells were concerned, results from two shape functions for bending were almost same except the neighbourhood of vertexes where slight differences were acknowledged, as shown in Fig. 4, where σ_m and σ_b denote the membrane and the bending stress, respectively.

In addition to the normal procedure given by Zienkiewicz [*6*], [*7*], another sim-

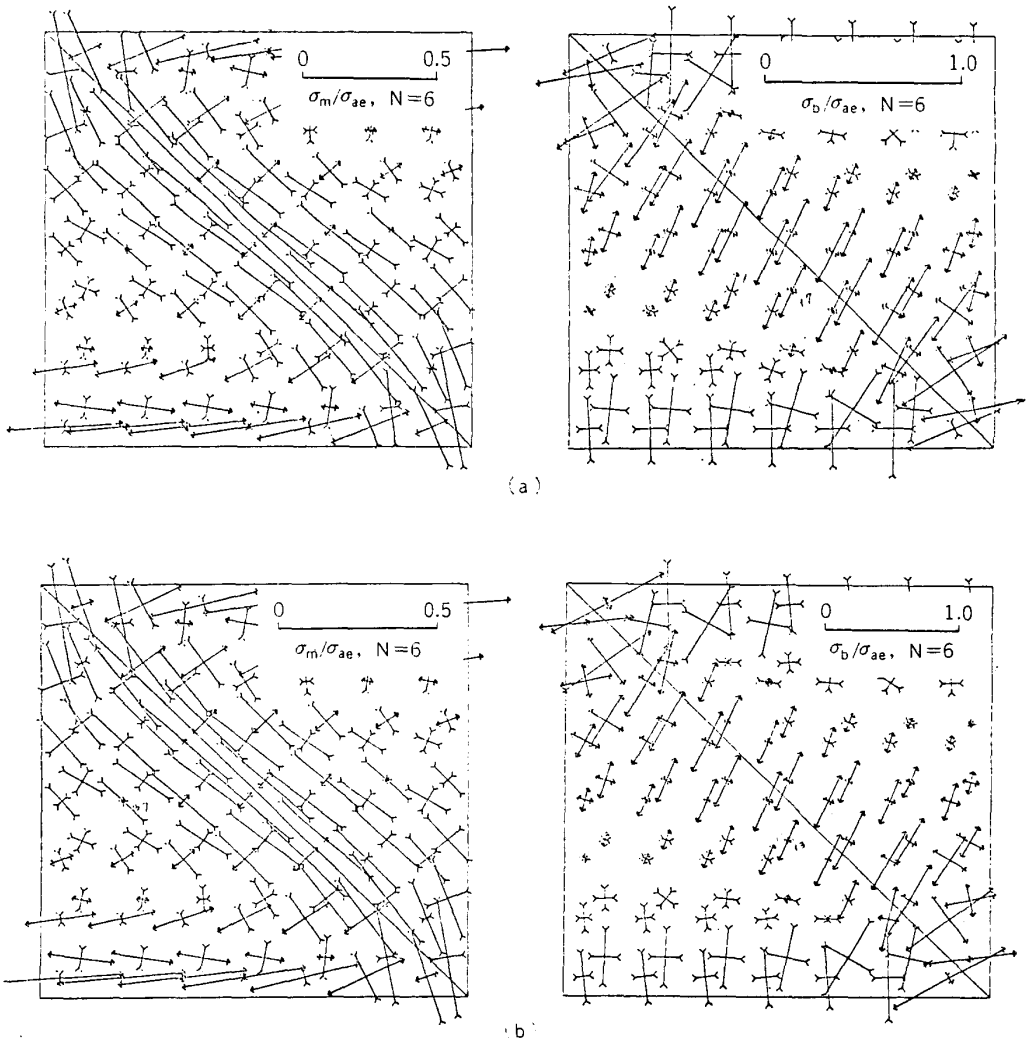

FIG. 4. Comparison between the non-conforming shape function (a) and the conforming one (b) on the stress level when PCCP shell is subjected to axial compression ($R/t=104$, $N=6$). The area of these displays corresponds to the square ABDC in Fig. 7.
σ_m: Membrane stress, σ_b: Bending stress, $\sigma_{ae}=P/2\pi Rt$.

plified method taken into account of a peculiar character of the *PCCP* shells was tried successfully. This method gave us same results in one third of the computing time. In this method, cylindrical coordinates were used and the omission of the bending rigidity in the radial direction were added in order to avoid solving the near-singular simultaneous equations.

4. Illustration and Comparison of Numerical and Experimental Results

4-1 Axial Compression

Fig. 5 shows the load-shortening curves of two kinds of *PCCP* shells. From this figure, the equivalent axial stiffness E_e which is defined as $E_e=Pl/(2\pi Rt\delta)$ is obtained.

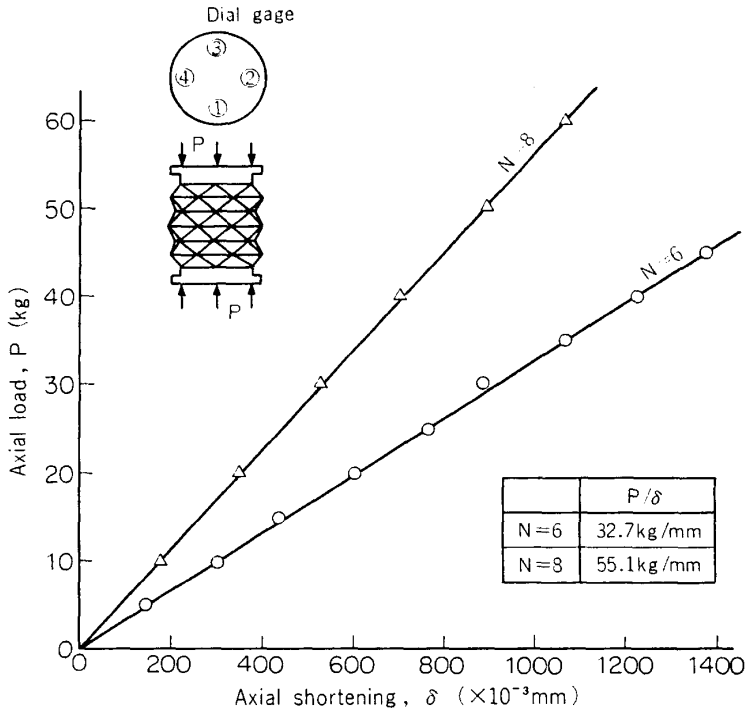

FIG. 5. Load-shortening curve of PCCP shells under axial compression.

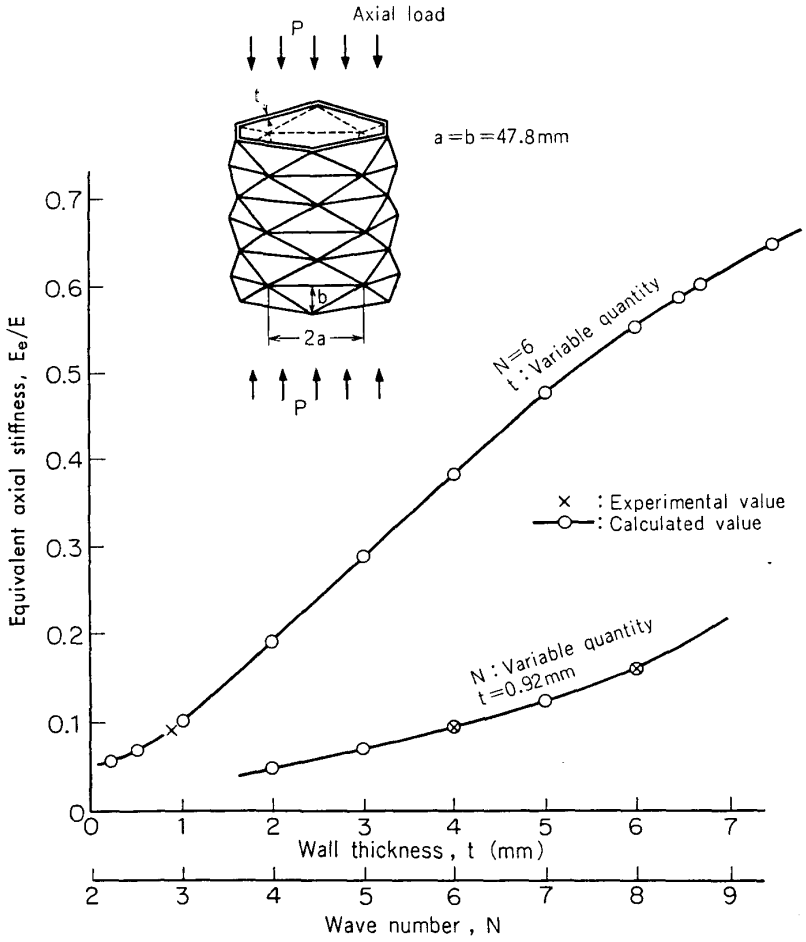

FIG. 6. Equivalent axial stiffness E_e/E for several values of wall thickness and the circumferential wave number.

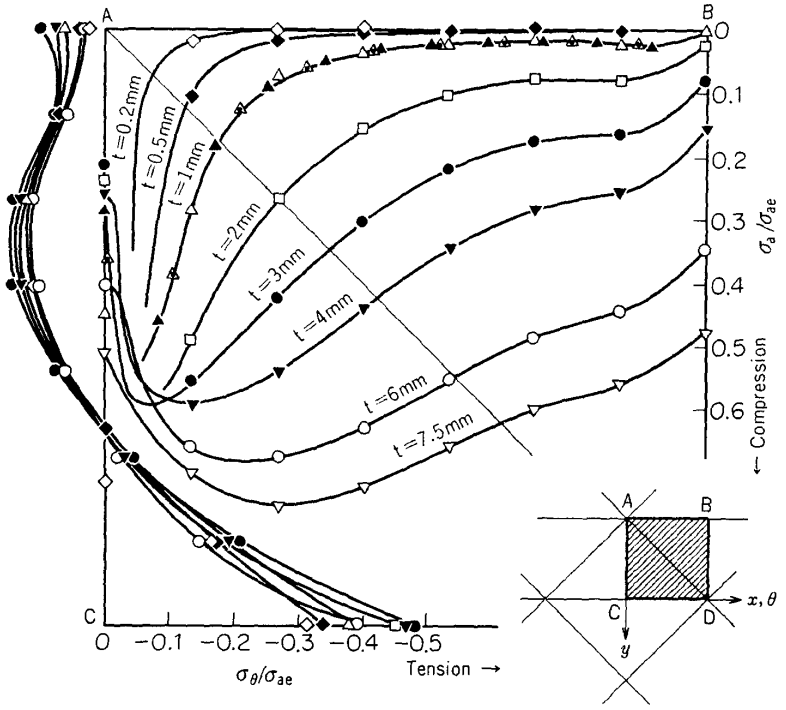

FIG. 7. Numerical reaction force distribution of PCCP shell ($N=6$), for several values of R/t under axial compression.
σ_a: Axial stress, σ_θ: Hoop stress, $\sigma_{ae}=P/2\pi Rt$. ◬ and ▲ correspond to the results in fine mesh.

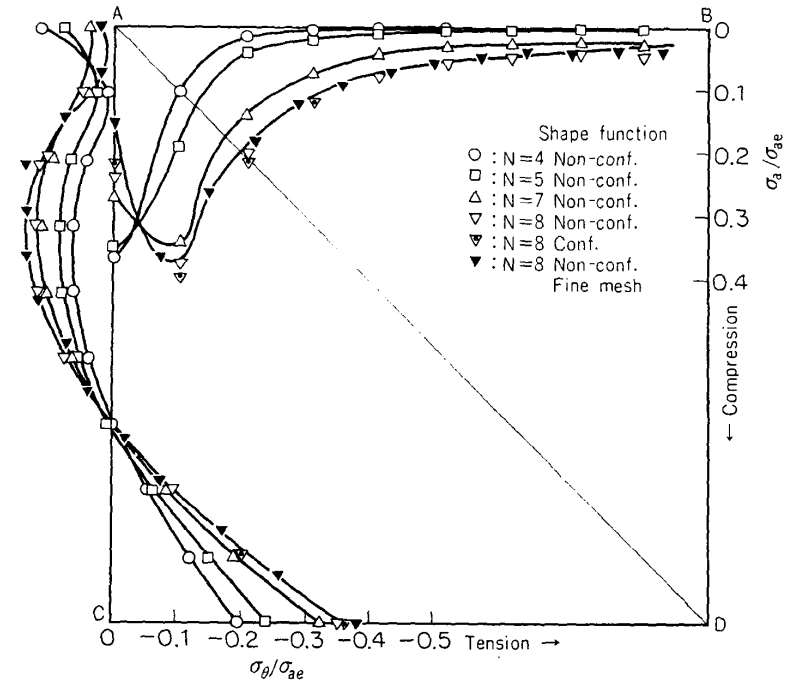

FIG. 8. Numerical reaction force distribution of PCCP shell ($R/t=104$) for several values of N under axial compression.
σ_a: Axial stress, σ_θ: Hoop stress, $\sigma_{ae}=P/2\pi Rt$.

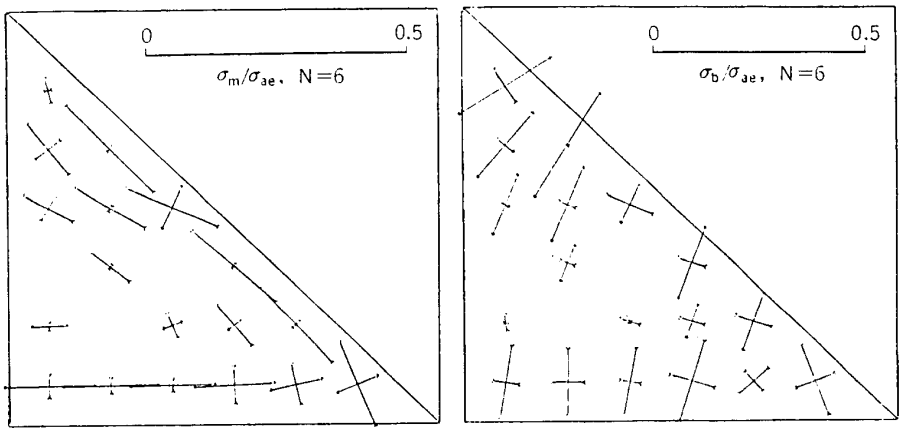

FIG. 9. Experimental stress distribution under axial compression ($R/t=104$, $N=6$). σ_m: Membrane stress, σ_b: Bending stress, $\sigma_{ae}=P/2\pi Rt$.

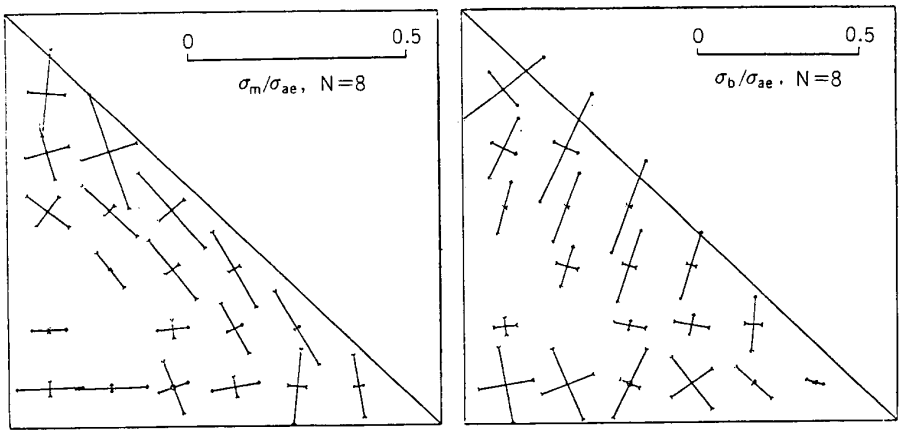

FIG. 10. Experimental stress distribution under axial compression ($R/t=104$, $N=8$). σ_m: Membrane stress, σ_b: Bending stress, $\sigma_{ae}=P/2\pi Rt$.

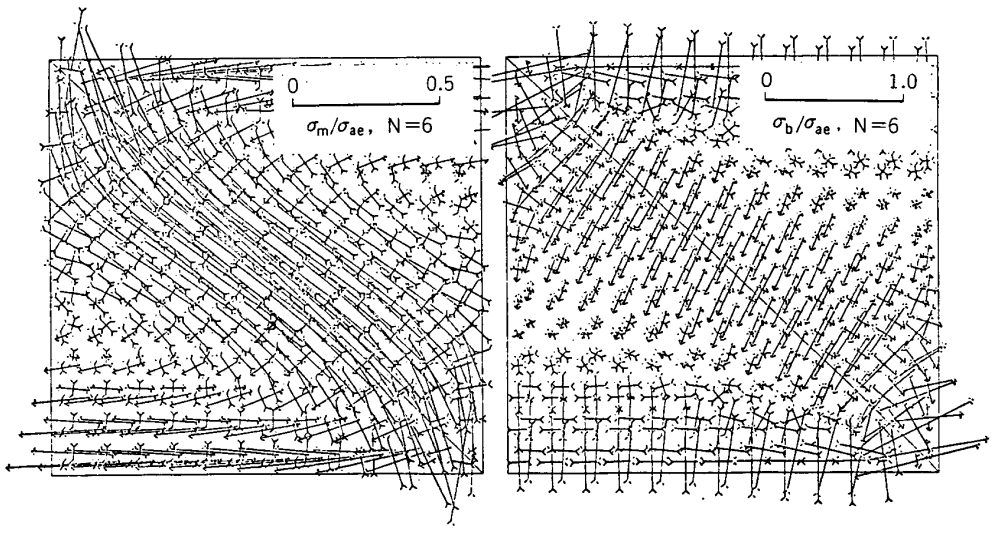

FIG. 11. Numerical stress distribution under axial compression ($R/t=104$, $N=6$). σ_m: Membrane stress, σ_b: Bending stress, $\sigma_{ae}=P/2\pi Rt$.

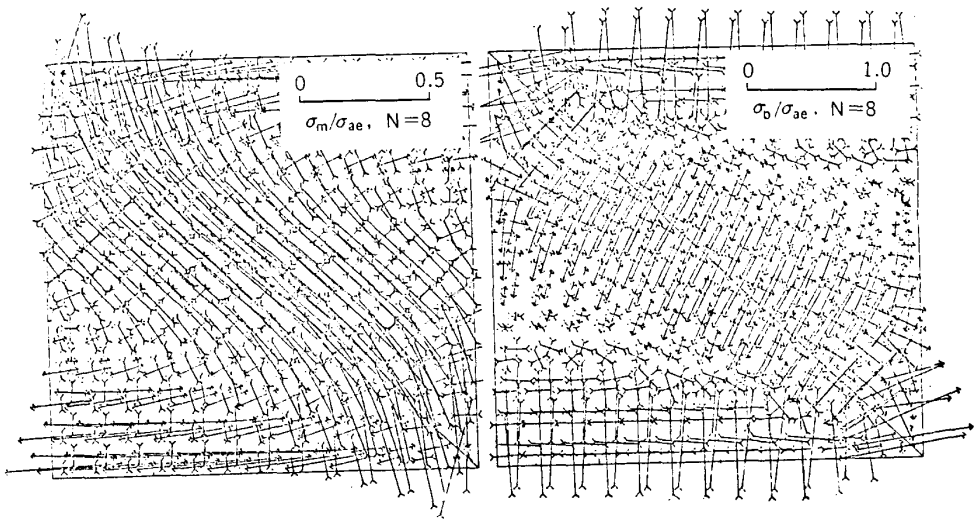

FIG. 12. Numerical stress distribution under axial compression ($R/t=104$, $N=8$). σ_m: Membrane stress, σ_b: Bending stress, $\sigma_{ae}=P/2\pi Rt$.

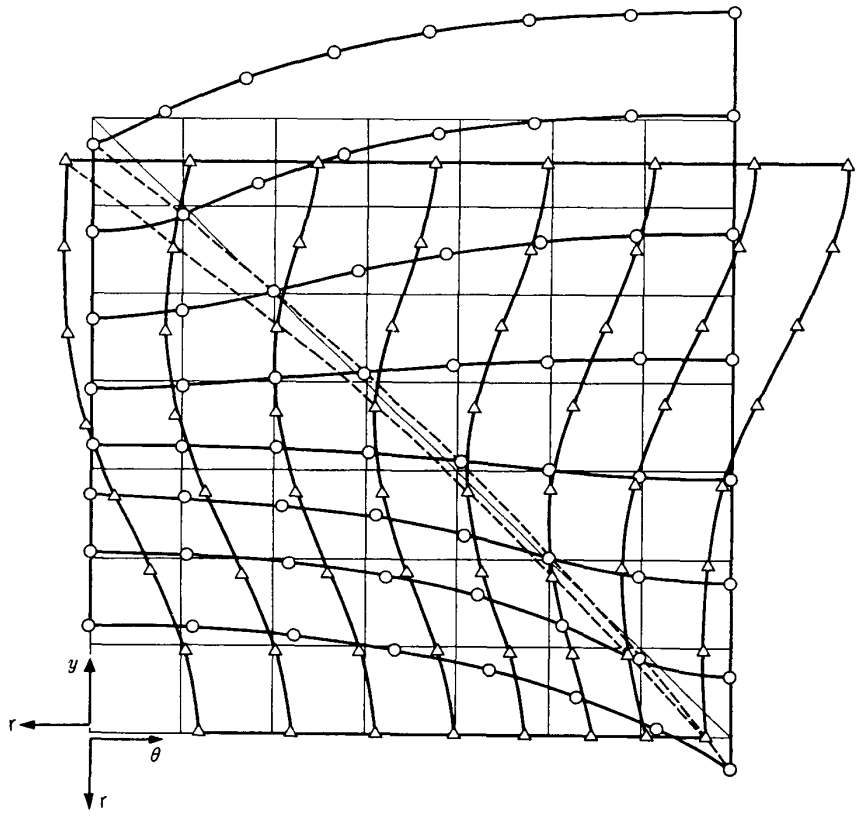

FIG. 13. Numerical displacement distribution of PCCP shell under axial compression ($R/t=104$, $N=6$). ○: (u_r, u_θ), △: (u_r, u_y).

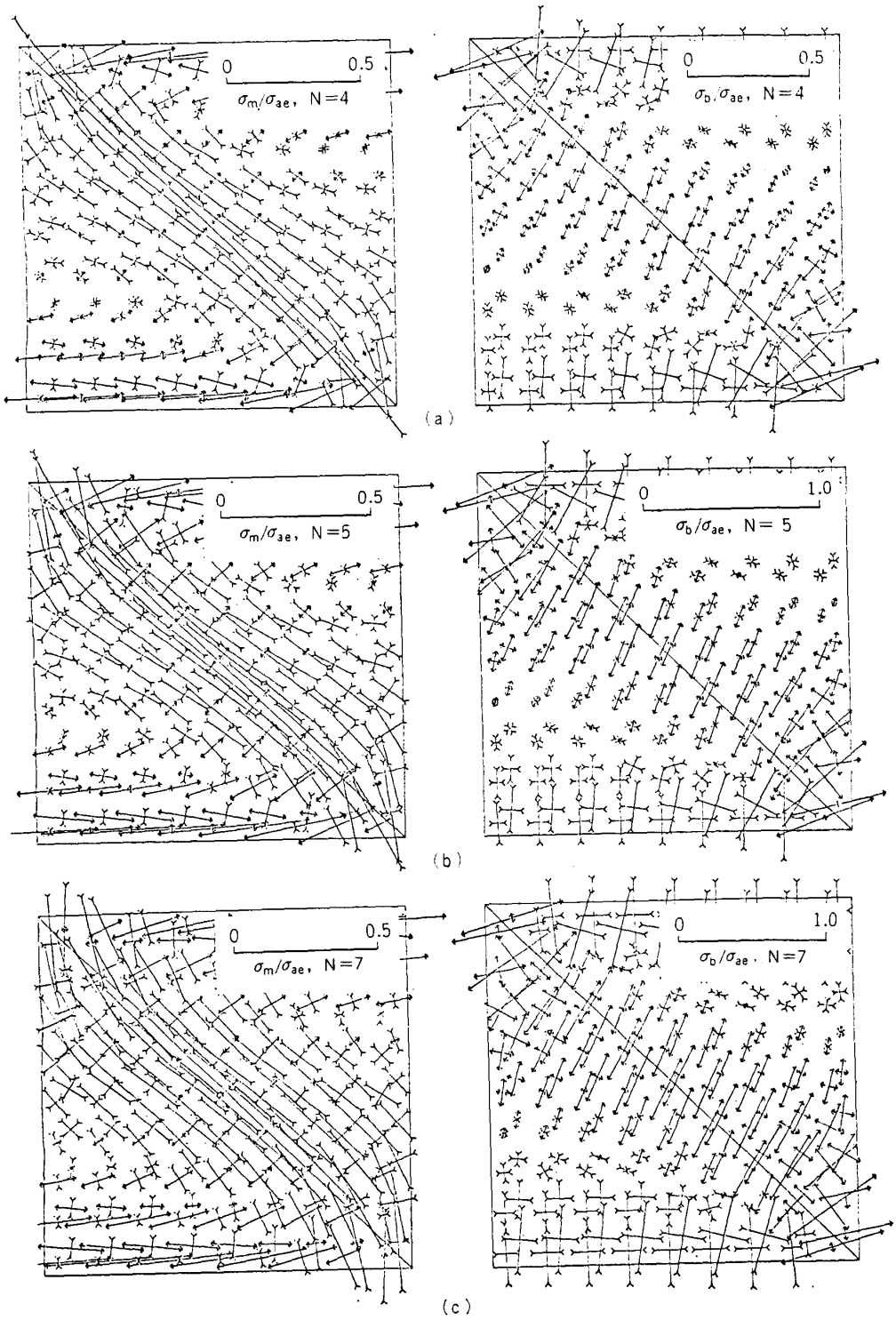

FIG. 14. Numerical stress distribution under axial compression for several values of N $(R/t=104)$.
σ_m: Membrane stress, σ_b: Bending stress, $\sigma_{ae}=P/2\pi Rt$.

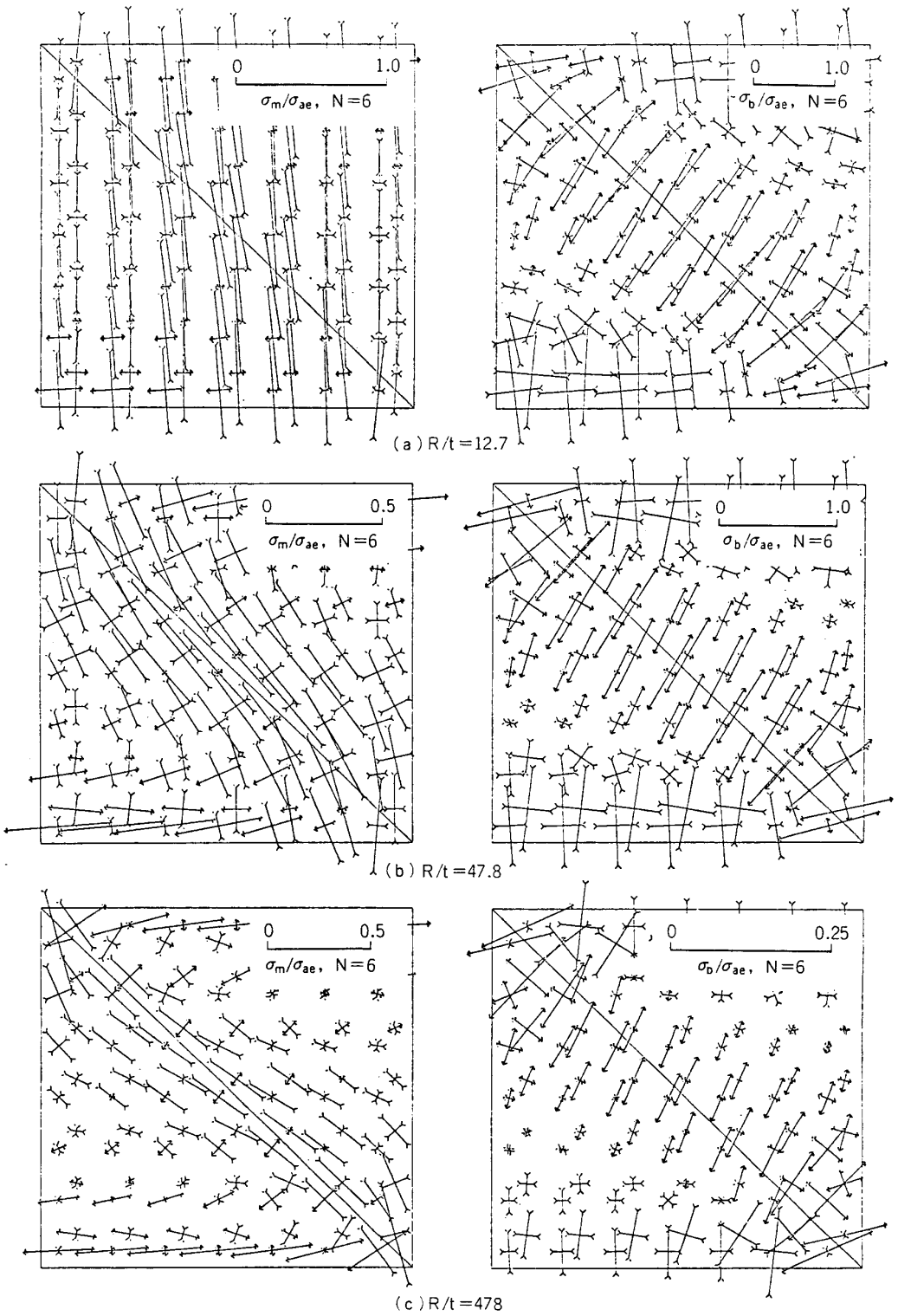

FIG. 15. Numerical stress distribution under axial compression for several values of R/t ($N=6$).
σ_m: Membrane stress, σ_b: Bending stress, $\sigma_{ae}=P/2\pi Rt$.

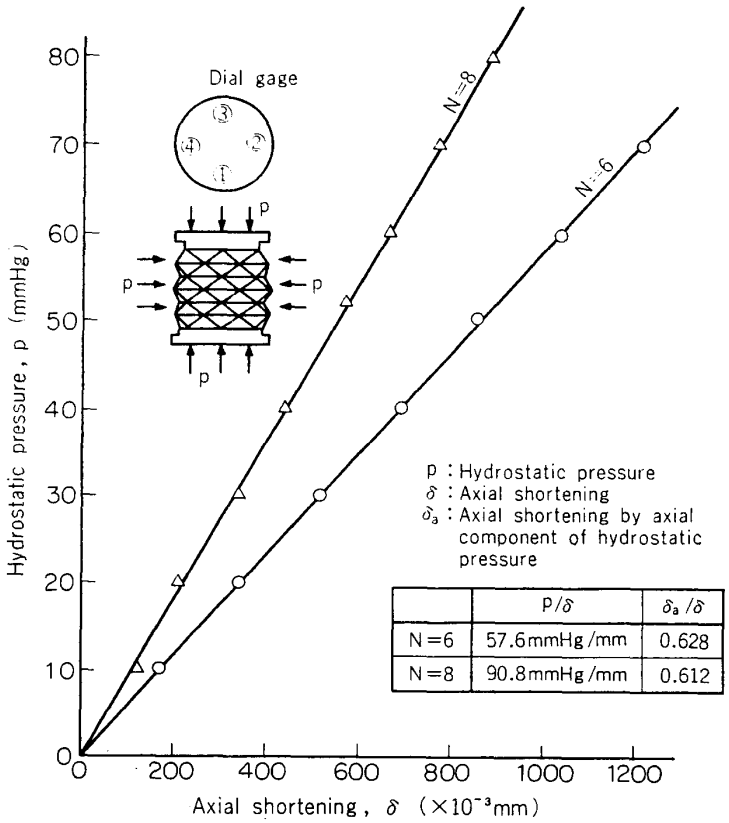

EIG. 16. Pressure-shortening curve of PCCP shells under hydrostatic pressure.

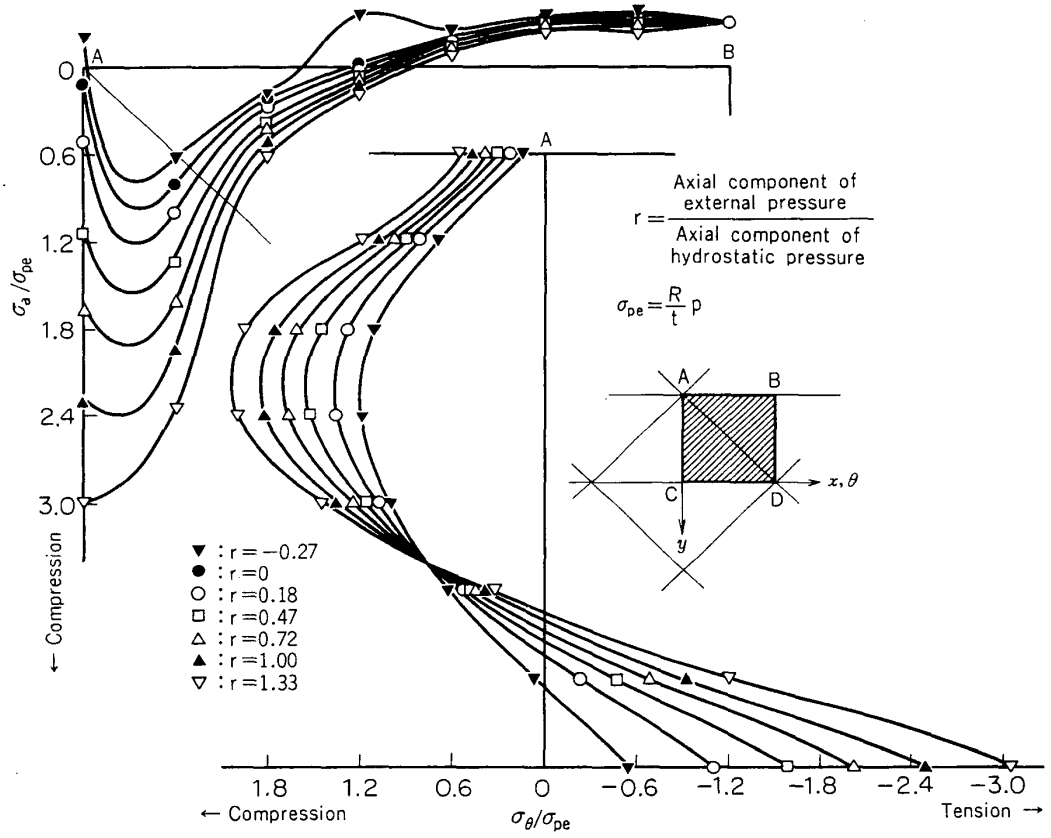

FIG. 17. Numerical reaction force distribution of PCCP shell ($R/t=104$, $N=6$) under several kinds of external pressures.
σ_α: Axial stress, σ_θ: Hoop stress, $\sigma_{pe}=pR/t$.

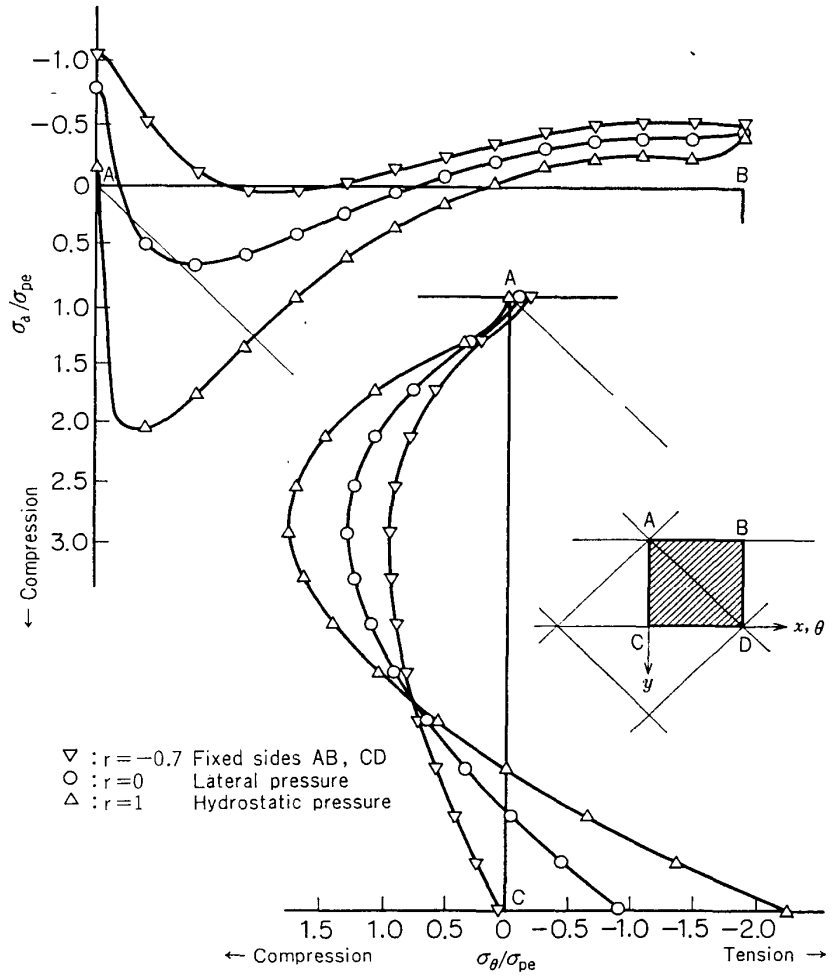

FIG. 18. Numerical reaction force distribution of PCCP shell ($R/t=104$, $N=8$) under several kinds of external pressures.
σ_a: Axial stress, σ_θ: Hoop stress, $\sigma_{pe}=pR/t$.

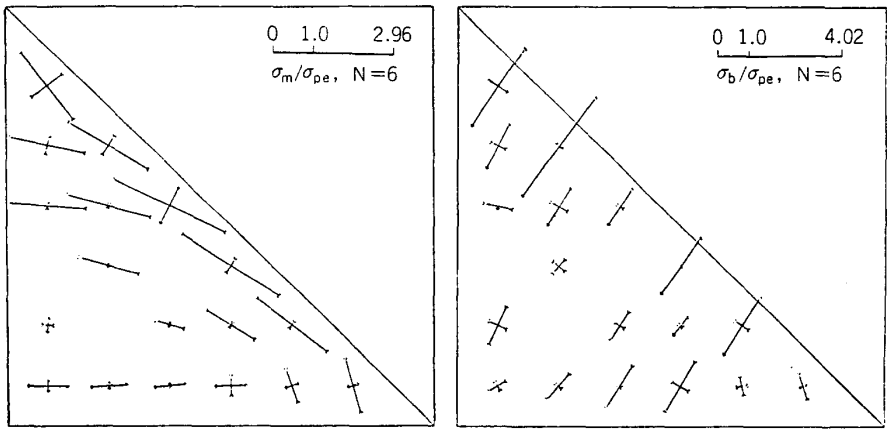

FIG. 19. Experimental stress distribution under hydrostatic pressure ($R/t=104$, $N=6$).
σ_m: Membrane stress, σ_b: Bending stress, $\sigma_{pe}=pR/t$.

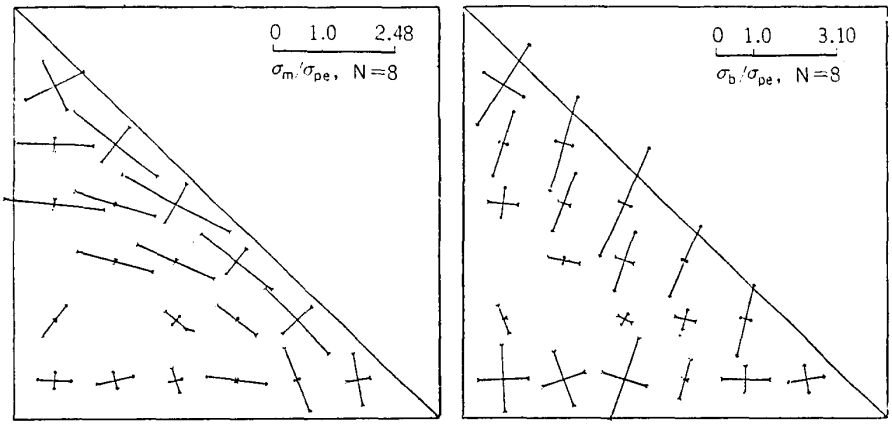

FIG. 20. Experimental stress distribution under hydrostatic pressure ($R/t=104$, $N=8$). σ_m: Membrane stress, σ_b: Bending stress, $\sigma_{pe}=pR/t$.

TABLE 2

	PCCP ($N=6$)	*PCCP* ($N=8$)	Cylinder (experiment)	Cylinder (Theory)
Axial fracture load	245 Kg	260 Kg	—	805 Kg
Hydrostatic fracture load	330 mmHg ~370 mmHg	234 mmHg ~240 mmHg	40 mmHg (buckle)	40 mmHg (buckle)

Here, P, l, R, t and δ denote the axial load, the axial length, the radius of the circum-cylinder, the wall thickness and the axial shortening related to the *PCCP* shell, respectively. The results are $E_e/E=0.093$ for $N=6$ and $E_e/E=0.150$ for $N=8$, where E is Young's modulus of the material of the *PCCP* shells and N is the circumferential wave number. In addition, the equivalent axial stiffness for several values of the quantities, t and N, are calculated numerically and illustrated in Fig. 6. The agreement between the experimental results and the numerical ones is good.

Numerical reaction force distributions are shown in Figs. 7 and 8, where σ_a and σ_θ denote the axial and the hoop normal stress of *PCCP* shells in cylindrical co-ordinates. Besides, σ_{ae}, which is defined as $\sigma_{ae}=P/(2\pi Rt)$, is the axial stress of the corresponding cylindrical shell subjected to the same loading.

Experimental stress distributions are shown in Fig. 9 for $N=6$ and Fig. 10 for $N=8$. Corresponding numerical stress distributions are shown in Figs. 11 and 12, respectively. Numerical nondimensional displacement distribution is shown in Fig. 13. Furthermore, numerical stress distributions for several values of R/t and N are shown in Figs. 14 and 15.

If we compare the numerical results shown in Figs. 11 and 12 with the corresponding experimental ones shown in Figs. 9 and 10, we find a close agreement in qualitative character. In quantitative character, however, the agreement is rather

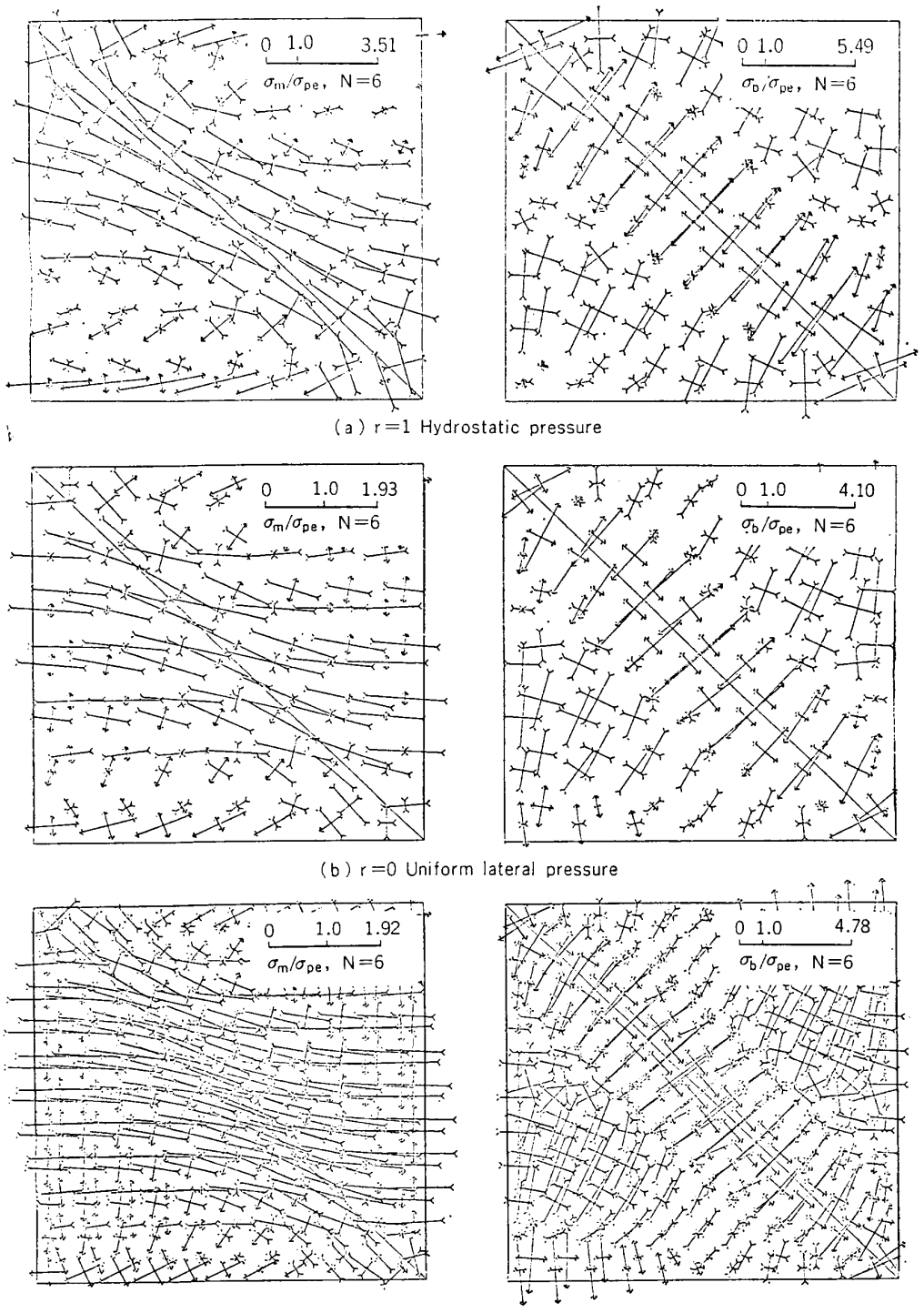

(a) r=1 Hydrostatic pressure

(b) r=0 Uniform lateral pressure

(c) r=−0.27 External pressure with restraint of the axial displacement

FIG. 21. Numerical stress distribution under several kinds of external pressures ($R/t=104$, $N=6$).
σ_m: Membrane stress, σ_b: Bending stress, $\sigma_{pe}=pR/t$.

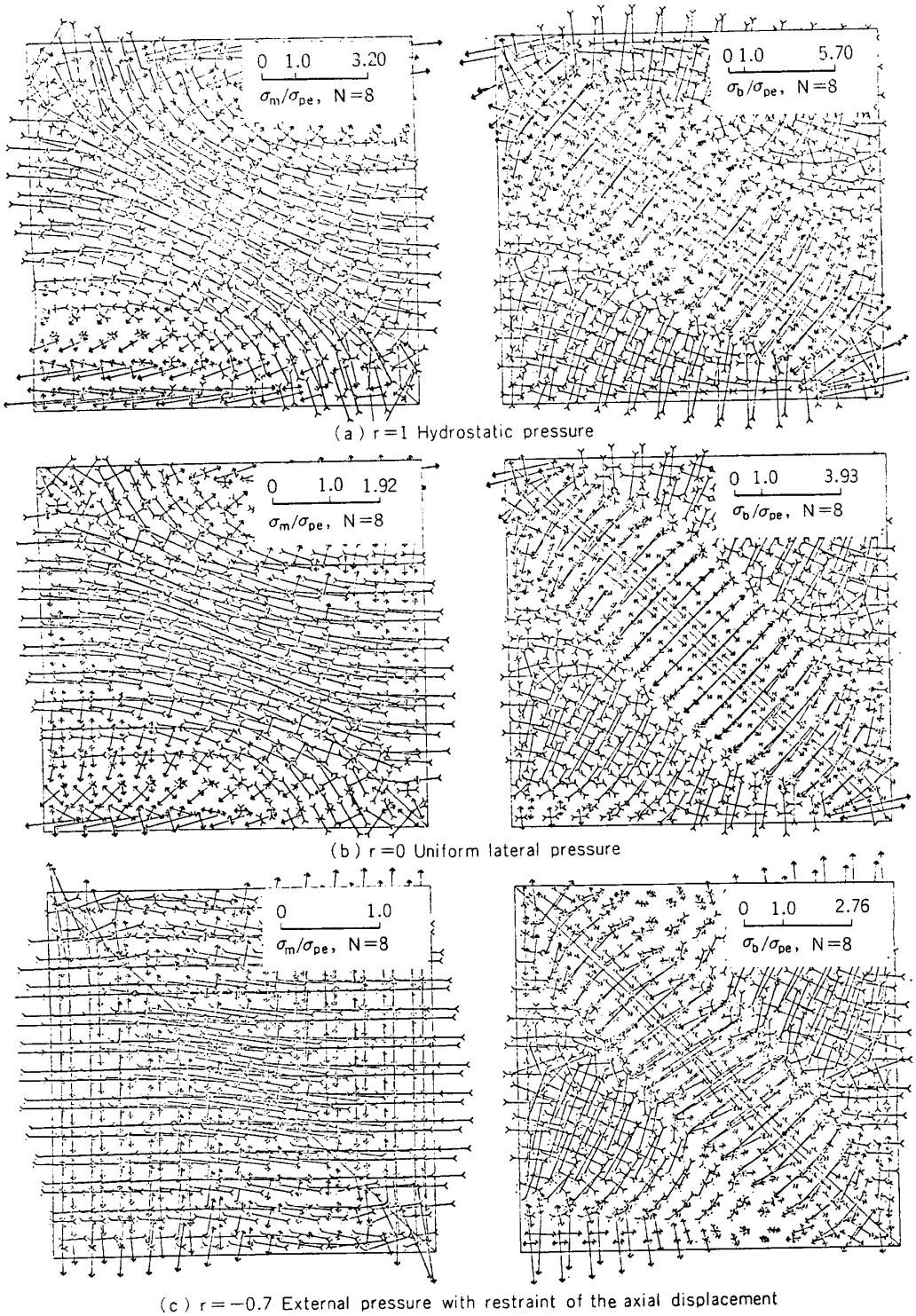

FIG. 22. Numerical stress distribution under several kinds of external pressures ($R/t=104$, $N=8$).
σ_m: Membrane stress, σ_b: Bending stress, $\sigma_{pe}=pR/t$.

poor. The ratio of the numerical result of the typical stress to the corresponding experimental one are about 1.3 in membrane stresses and about 2.0 in bending. More detailed research is necessary with regard to this difference.

4-2 *Hydrostatic pressure*

Fig. 16 shows the pressure-shortening curves of two kinds of *PCCP* shells. From Figs. 5 and 16, we can estimate the axial shortening of the *PCCP* shell subjected to the coupled loading condition with hydrostatic pressure and the axial load. Numerical reaction force distributions are shown in Figs. 17 and 18, in which σ_{pe} is defined as $\sigma_{pe}=pR/t$, where p denotes the value of the external pressure, and corresponds to the hoop stress of the cylindrical shell under the same loading.

Experimental stress distributions are shown in Figs. 19 and 20 for $N=6$ and 8, respectively. Numerical stress distributions for several values of r, which is defined as the ratio of the axial component of the external pressure to the one of the hydrostatic pressure, are shown in Figs. 21 and 22 for $N=6$ and 8, respectively.

In a comparison between the numerical results and the experimental ones, we find a close agreement in qualitative character. In quantitative character, however, the ratio of the numerical result of the typical stress to the corresponding experimental one are about 1.2 in membrane stresses and 1.6 in bending. In Table 2, the critical axial loads and the critical hydrostatic pressures at which *PCCP* shells fractured are listed.

5. Behaviour of PCCP Shell in Elastic Region

5-1 *Axial Compression*

The resultant stress distributions shown in the previous chapter have vividly revealed the primary and some extraordinary characteristics of *PCCP* shells subject to axial loading.

The membrane stress distributions can be described that as if the stress flows within the bands along ridge lines as shown in Figs. 14 and 15. The compressive stress appears in the vicinity of convex and thus oblique ridges and, on the contrary, the tensile stress appears in the vicinity of concave circumferential ridges. In the vicinity of the centroid of the triangular element, the stress is small and the principal directions are ambiguous. Such stress pattern shows striking resemblance to the force distribution of a hypothetical framed structure whose frame replace each ridge line of the corresponding *PCCP* shell. This tendency, as expected, becomes pronounced as either the thickness t or the wave number N decreases. On the contrary, as either t or N increases as shown in Figs. 14 and 15, membrane stresses distribute more and more uniformly.

Bending stresses also concentrate within the bands along ridge lines. If we take the positive bending stress as the one exhibits tensile stress on the outer surface of the shell, the positive and negative bending stresses appear along the convex and concave ridges, respectively. In both cases, the directions of larger principal stresses cross the ridge lines.

From the other point of view, the bending stresses are such that they distribute along every ridge so as to advance the "folding" process of this folded plate structure. This character is important in relation to the collapsing mechanism of cylindrical shell as suggested by Miura [*8*]. It is also very interesting to note that the direction of the band where positive bending stresses are prevalent intersects the oblique ridge lines at a certain angle, say as much as 20 degrees (see Fig. 14). This feature is the key fact that provides the sound basis for the Miura's hyphothesis on collapsing mechanism of cylindrical shells [*8*].

5-2 Hydrostatic pressure

The membrane stress distributions for the uniform hydrostatic pressure are such as shown typically in Figs. 21 and 22. Surprisingly, in spite of its uneven shape, the membrane stresses for *PCCP* shells are not much different from those of the circular cylindrical shells. This may be explained in an approximate manner as follows: the hoop stress for an end-closed cylinder-like shall is the primary stress which is about twice as much as the axial stress and the any circumferential cross section of this concave polyhedral shell is ironically a convex polygon inscribing a circle. This tendency, as expected, becomes more pronounced as either the thickness t or the wave number N increases.

The bending stress distribution is like that shown typically in Figs. 21 and 22. These patterns closely resemble what appears in the rhombic plate fixedly supported at boundaries and subjected to a lateral pressure. The bending stress is highly concentrated at edges. When the axial displacement is restricted by some means, the stress decreases considerably.

6. Behaviour of PCCP Shell under Extreme Loading

6-1 Plastic Deformation Obserbed in Axial Compression

The *HIPS* sheet, which is usually half-transparent, has the property that the region where the deformation exceeds a certain limit of deformation turns opaque. The use of this phenomenon provides us a unique mean to study the advance of plastic deformation under increasing load.

Fig. 23 is one of the photos of such an experiment and it corresponds to the last stage, that is, the fractured specimen. Due to the illumination of taking photos, the part turned opaque is seen black shaded in this photo. The plastic deformation initiates at the vicinity of vertexes and then proceeds to concave ridges. This result is consistent with the result of the elastic stress analysis in the preceding chapters.

6-2 Buckling of PCCP Shell under Hydrostatic Pressure

The plastic deformation initiates at the vicinity of oblique ridges and then appears at centroids of triangular elements. This results is consistent with the results of the elastic stress analysis in the preceding chapters.

In the final stage, the *PCCP* shell for $N=6$ failed explosively and was broken to

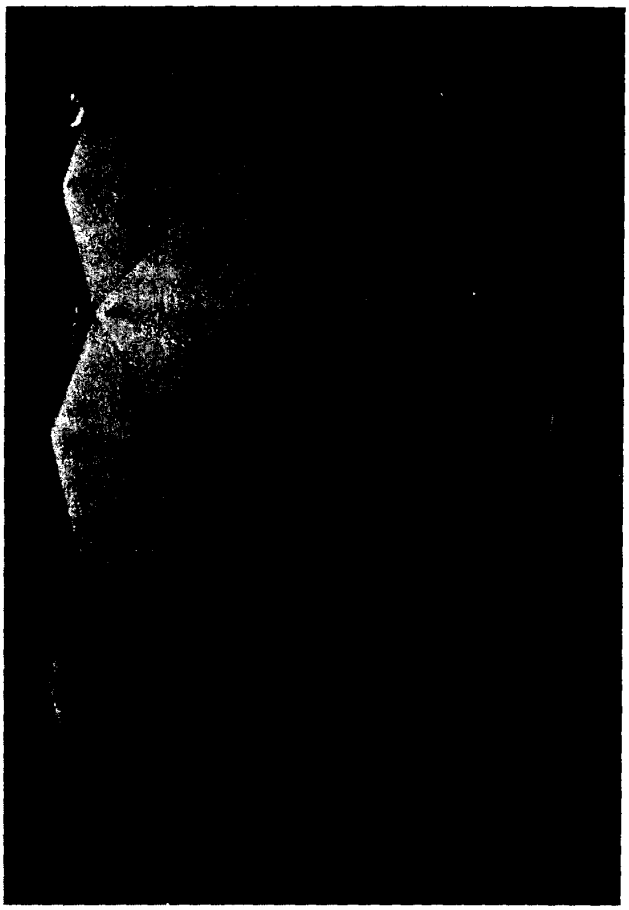

FIG. 23. The fractured PCCP shell ($N=6$) in axial compression.

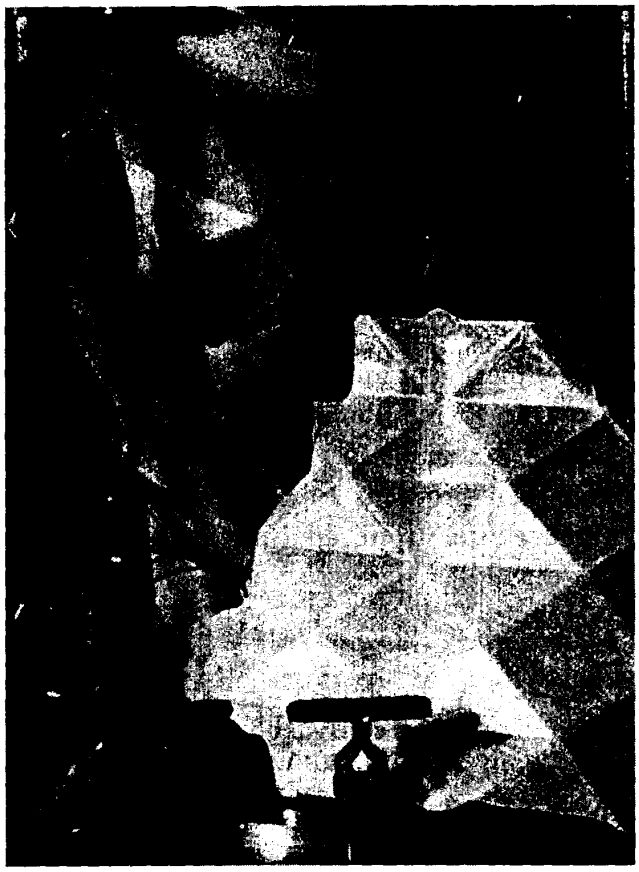

FIG. 24. The fractured PCCP shell ($N=8$) under hydrostatic pressure.

pieces. However, the one for $N=8$ seemed to buckle first and then to fail catastrophically. From the fractured specimen, as shown in Fig. 24, we could find the interesting buckling mode where the shell surface displaced to a cylindrical surface. In the case of the circular cylinder, it buckled first and then fractured after the lapse of a short time by maintaining the critical pressure. The critical hydrostatic pressures of three types of shells are shown in Table 2.

As is evident from this table, the critical pressures for the *PCCP* shells are very high in comparison with the one for the cylindrical shell. Therefore, we will be able to expect the potentiality of *PCCP* shells as the underwater structure.

7. Conclusions

In this study, we have obtained the following conclusions.

1) Both the numerical and the experimental analytical methods are presented in order to investigate *PCCP* structures.

2) Elastic behaviours and stress distributions of *PCCP* shells subjected to either axial compression or hydrostatic pressure are made clear.

3) The instability of *PCCP* shells subjected to hydrostatic pressure is studied experimentally. The higher buckling pressures of *PCCP* shells in comparison with that of the circular cylinder gives support to the use of the *PCCP* shell structure as an underwater habitat as suggested by Knapp.

4) The particular stress distribution observed in *PCCP* shells subject to axial compression gives a basis for Miura's hypothesis to explain the collapsing mechanism of general cylindrical shells. Resultantly, the study of *PCCP* shell is closely relating to the collopsible shock energy absorbing structure.

Acknowledgement

The authors wish to thank Mr. Masamori Sakamaki and Mr. Kuniyoshi Minami for their helpful collaboration.

Department of Aerodynamics
Institute of space and Aeronautical Science
University of Tokyo
February 27, 1975

References

[*1*] Miura, Koryo, "Proposition of Pseud-Cylindrical Concave Polyhedral Shells," Report No. 442, Vol. 34, Institute of Space and Aeronautical Science, Univ. of Tokyo, Nov., 1969.

[*2*] Miura, Koryo, "Proposition of Pseud-Cylindrical Concave Polyhedral Shells," Proc. IASS Symposium on Folded Plates and Prismatic Structures, Wien, Sept. 1970.

[*3*] Knapp, R. H., "Proposal of Thesis in Partial Fulfillment of the requirements for the

Ph.D in Ocean Engineering," Department of Ocean Engineering, Univ. of Hawaii, 1971.

[*4*] Bazeley, G. P., Cheung, Y. K., Iron, B. M. and Zienkiwicz, O. C., "Triangular Elements in Plate Bending Conforming and Nonconforming Solutions," Proc. Conf. on Matrix Methods in Struct. Mech., Air Force Inst. of Tech., Wright Patterson A. F. Base, Ohio, 1965.

[*5*] Clough, R. W. and Tocher, J. L., "Finite Element Matrices for Analysis of Plate in Bending," Proc. Conf. on Matrix Methods in Struct. Mech., AFFDL-TR-66-80, 1966.

[*6*] Zienkiewicz, O. C. and Cheung, Y. K., "The Finite Element Method in Structural and Continuum Mechanics," Mc Graw Hill, 1967.

[*7*] Zienkiewicz, O. C., The Finite Element Method in Engineering Science, Mc Graw-Hill, 1971.

[*8*] Miura, Koryo, "Collapsing Mechanism of Prismatic Structures," 23th. Japan National Congress for Applied Mechanics 1973 or Bulletin of the Institute of Space and Aeronautical Science, Univ. of Tokyo, Vol. 10, No. 4(B), 1974.